

Integrating fine root diameter and watershed mapping to characterize rhizosphere hydrology



Jeffrey M. Warren ^{a,*}, Keita F. DeCarlo ^{b,f}, Hassina Bilheux ^c, Jean-Christophe Bilheux ^c, Kelly Taylor ^{d,e,f}

^a Environmental Sciences Division, Oak Ridge National Laboratory, Oak Ridge, TN, 37831, USA

^b National Minerals Information Center, United States Geological Survey, Department of Interior, USA

^c Neutron Scattering Division, Oak Ridge National Laboratory, Oak Ridge, TN, 37831, USA

^d Department of Geography, University of California, Santa Barbara, CA, 93106, USA

^e Bren School of Environmental Science & Management, University of California, Santa Barbara, CA 93106, USA

^f Department of Civil & Environmental Engineering, Princeton University, Princeton, NJ 08544, USA

ARTICLE INFO

Keywords:

Digital image processing

Neutron imaging

Root traits

Root water uptake

Soil hydrology

ABSTRACT

Root morphology and soil hydraulic characteristics were integrated using watershed distance mapping to show water distribution and uptake across the plant-soil interface. Poplar (*Populus deltoides*, *P. trichocarpa*), maize (*Zea mays*), juniper (*Juniperus virginiana*), grape (*Vitis rotundifolia*) and maple (*Acer saccharum*) seedlings were grown in sand, after which root diameter and soil water dynamics were assessed via sequential neutron radiography. Three local soil regions (root-soil interface or edge, rhizosphere, bulk soil) were classified based on both radial distance from the root surface and diameter of the nearest root, from which changes in water content and distribution were characterized using digital image processing. Water content dynamics across the rhizosphere showed two different species-independent processes: a consistently elevated water content at the root-soil edge interface which increased with root diameter, and hysteresis as the rhizosphere transitioned to bulk soil (~0.5 cm from the root), independent of root diameter. Water uptake per unit root surface area declined exponentially with root diameter, independent of species. Results highlight the species-independent hydrologic characteristics of the rhizosphere and the potential for evaluating them in a local spatially connected soil context. Avenues for improved integration of soil and root characteristics are discussed.

1. Introduction

The fundamental aspects of plant water uptake span morphological, physiological and functional responses to soil water availability. A key mediator of this plant-soil dynamic is the region of soil immediately adjacent to the root, known as the rhizosphere (Hiltner, 1904; Hartmann et al. 2008). The rhizosphere is formed via root penetration through the soil, root release of water and exudates and subsequent growth of microbial and bacterial communities (Gregory, 2006; Hinsinger et al. 2009) – a process that can also affect (or be affected by) soil compaction near the root (Dexter, 1987; Aravena et al., 2014; Koebernick et al. 2017). The rhizosphere's sphere of influence is defined in context of the specific processes involved and their spatial scale: free-living microbial activity is limited to the sub-mm scale, while impacts on water and solute flux can be greater, at the cm + scale (Darrah, 1993; York et al.,

2016).

Despite the relatively limited scale of root influence on the soil, the rhizosphere has biological, chemical and physical properties that are often much different from that of bulk soil. One component is rhizosphere hydraulic plasticity – a spatially and temporally dependent behavior in response to soil water availability (Carminati et al. 2011; Carminati and Vetterlein, 2013) that has been suggested to reduce plant hydraulic stress during drying conditions (Nazari et al. 2022). This plasticity is largely a function of fine root exudation, including low molecular weight primary metabolites (Canarini et al. 2019) and higher weight polysaccharides in a hydrated mucilage that can act as a surfactant or hydrogel to alter the water retention characteristics in the rhizosphere (Moradi et al. 2012; Ahmed et al. 2016b; Naveed et al. 2019). Eventually decaying and becoming hydrophobic, mucilage creates shrinkage-induced void spaces as the soil dries that can reduce

* Corresponding author. Environmental Science Division Oak Ridge National Laboratory Oak Ridge, TN, 37831, USA.

E-mail address: warrenjm@ornl.gov (J.M. Warren).

root-soil connectivity and the ability for rapid root water uptake following wetting (Carminati et al. 2009; Ahmed et al. 2018a; Zarebanadkouki et al. 2018). Mucilage increases soil aggregation and porosity and changes pore size distribution, which can affect soil water retention characteristics (Whalley et al. 2005; Feeney et al. 2006; Hallett et al. 2003). Chemical quality of exudates and root distribution and turnover have also been linked to macroaggregate development (Poirier et al. 2018). In addition to roots and mycorrhizal hyphae (Dhiman et al. 2018; Marcacci et al. 2022), these processes all have impacts on soil hydraulic properties that are likely as dynamic as the root system itself. Consequently, experimental results of rhizosphere water retention can show seemingly contradictory results, with water content and uptake in the rhizosphere shown to be either lower (MacFall et al. 1990; Segal et al. 2008) or higher (Nakanishi et al. 2005; Tumlinson et al. 2008; Moradi et al. 2011) than the bulk soil with different species and under different experimental conditions.

Root exudate characteristics can also vary with plant species, manifesting themselves not only in spatial heterogeneity in the radial dimension away from the root, but also in the lateral dimension along the root as it grows. For example, in leguminous species like lentils, exudate deposition is uniform along the root, while maize exudate deposition is concentrated at the root tip (Razavi et al. 2016). In maize, water uptake switches from laterals of seminal roots to crown roots as the roots mature and develop in size (Ahmed et al. 2018b). In lupine species, water uptake has been shown to be higher in the upper half of the root system and progressively lower along individual roots from the younger distal to older proximal sections (Zarebanadkouki et al. 2013, 2014). Water uptake dynamics vary by root order and size (Rewald et al. 2011; Dhiman et al. 2018) supporting the need to define fine roots not just by size (*i.e.*, < 2 mm) but by their functional type, *e.g.*, absorptive versus transportive (McCormack et al. 2015).

Rhizosphere properties reflect the intertwined relationships in soil-plant resource exchanges with inflow of water and nutrients and outflows of mucilage and exudates and indicate the importance of evaluating them concurrently. Rhizosphere research has often centered on root and microbial interactions with less focus on the physical soil properties (Gregory and Hinsinger, 1999; Gregory, 2006). A research framework that spatially and temporally integrates the intersection of roots and the adjacent soil can improve understanding of the rhizosphere. Image-based methods can capture these dynamics at the root-soil interface and illustrate influences of root order, age, prior plant stress or morphology on water uptake (Dhiman et al. 2018; Daly et al. 2018). Imaging can reveal root system architecture (RSA) and root-specific functional linkages to the soil can be established using various image processing techniques, such as distance transforms (Koebernick et al. 2014; Schlüter et al. 2018). Experimental data can then be used to inform root-soil rhizosphere modeling advances to understand how functional processes work across scales (Roose et al., 2016, Schnepf et al. 2022). Various imaging techniques can reveal *in situ* processes at the root-soil interface, and include light transmission (Garrigues et al. 2006), optical fluorescence imaging (Rudolph Mohr et al., 2014, 2021), X-ray (Koebernick et al. 2017; Daly et al. 2018), NMR (Pohlmeier et al. 2013) and neutron imaging (*e.g.*, Oswald et al. 2008; Carminati et al. 2010; Warren et al. 2013, Zarebanadkouki et al. 2016; Dhiman et al. 2018). Neutron imaging is an ideal method for analyzing local spatially- and temporally dependent root-soil structural and hydraulic processes in the rhizosphere due to its high resolution (tens of microns) and image acquisition time on the order of seconds (Cai et al., 2022). Combined with high neutron sensitivity to hydrogen, and thus water, neutron radiography allows for the analysis of the interplay between root morphology and soil water distribution and dynamics. These dynamics are readily visualized using sequential neutron imaging over time, *e.g.*, Video S1 shows maize root uptake of deuterium oxide (used to enhance contrast) following injection beneath the deepest roots.

Supplementary video related to this article can be found at <https://doi.org/10.1016/j.rhisph.2023.100738>

The primary objective of this study was to simultaneously quantify *in situ* fine root architecture, morphology and soil/water dynamics in the rhizosphere (*i.e.*, water content or uptake in context of spatial distance around the root). Given results in prior studies of links between rhizosphere soil water dynamics and root age/morphology (*e.g.*, Rewald et al. 2011; Zarebanadkouki et al. 2014; Ahmed et al. 2018b; Dhiman et al. 2018) we hypothesized that patterns of water content in the rhizosphere and apparent root water uptake rates may be similar across species for the same diameter of roots when evaluating them by order of spatial proximity of roots and soil, and changes in soil water content over time. While recent studies have used distributions of soil distance to the nearest root surface to characterize root system architecture (RSA; Schlüter et al. 2014), this study further leveraged the spatial relationships between each soil pixel and root surface pixel to assess the root to soil hydraulic interconnectivity of the interface. To that end, digital image processing of sequential neutron radiographs was used to analyze multiple plant species growing in sand to characterize relationships between root size, rhizosphere water content and root water uptake.

2. Materials and methods

2.1. Plant material and treatments

To address if there were species-independent relationships between root size and rhizosphere water dynamics, we leveraged prior and new experiments at the beamline to broaden species diversity. We used six different species with widely varying root traits and functional types, but overlapping root sizes, including an evergreen tree, three deciduous trees, a woody vine and a grass. Eastern red cedar or juniper (*Juniperus virginiana* L.), poplars (*Populus deltoides* W. Bartram ex Marshall, *Populus trichocarpa* Torr. & A. Gray ex Hook) sugar maple (*Acer saccharum* Marshall), grape (*Vitis rotundifolia* Michx.) and maize (*Zea mays* L.) plants were grown from seed or transplanted into rectangular aluminum containers (20 × 18 × 1.2 cm, interior size 19 × 17.6 × 1.0 cm) and propagated for later neutron imaging experiments. Samples were prepared in advance of planned beamtime, or based on their availability when beamtime became available (*e.g.*, rescheduled due to logistics, technical issues). Various species had different initial propagation, but all were then established between layers of sand in sample containers and grown so that a rhizosphere had time to develop. Sand was used to minimize the confounding factors associated with neutron imaging of finer textured or organic soils, whose hydrogen concentration (and subsequent neutron cross-section) is not solely dependent on water content.

The *P. trichocarpa* sample was grown from seed in sand and then transplanted into the aluminum containers after 5 weeks (Dhiman et al. 2018). *P. deltoides* clonal samples were propagated from cuttings using a hydroponic system, then after one month were transplanted into the aluminum containers. For the *Z. mays* samples, seeds were soaked in water for 2 days, germinated in a Petri dish on moist paper towels for one week, then transplanted into the containers with the kernel at or just below the sand surface. One-year-old seedlings of *V. rotundifolia*, *J. virginiana* and *A. saccharum* samples were collected at or nearby the Oak Ridge Reservation, then transplanted into the aluminum containers. Transplanted plant roots were carefully rinsed in water, displayed in between moistened layers of silica quartz sand (0.3–0.6 mm grain size; fully characterized in Cheng et al. 2012; Kang et al. 2013, 2014) and inundated with water amended with balanced N:P:K and micronutrients to fully settle roots into the sand; hereafter referred to as soil. Once packed, the top and bottom of the containers were sealed with tape to limit evaporation and propagated in an onsite growth chamber at 20–25 °C with 17.5 h day cycle (Warren et al. 2013) for imaging 1–5 weeks later (Fig. 1a). During their time in the containers, plants were watered periodically based on mass-based water use, every 1–3 days; apparent transpiration varied with plant size and density, ranging from ~1 to 18 ml per day. The plants adapted to the containers well, with variable axial fine root growth ranging from 0.15 to 0.65 cm per day (*e.g.*, Warren et al.

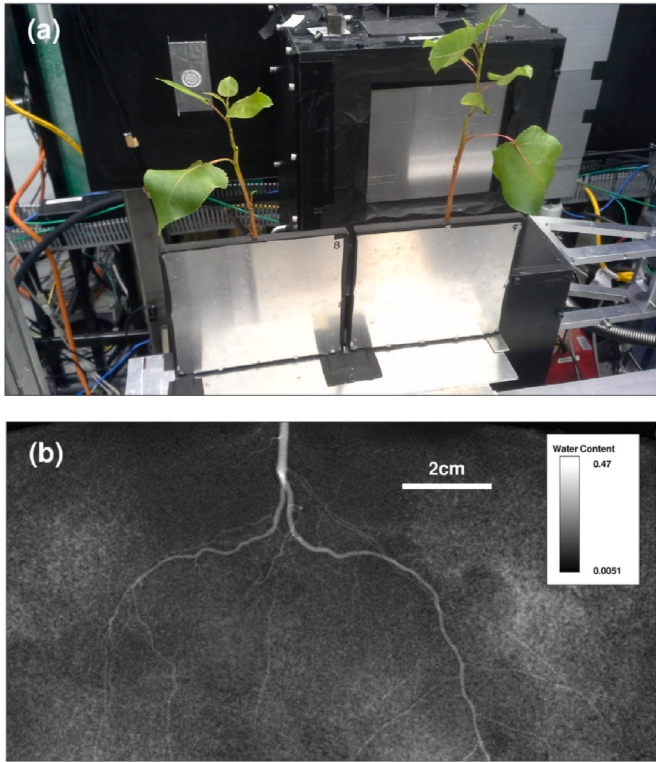


Fig. 1. (a) Experimental set up with two poplar ramet plant systems on an automated lift table in front of the detector. (b) neutron attenuation radiograph of a water content map of a poplar root system (grown from seed) in sand.

2013). The age of the rhizosphere around individual roots ranged from <1 day for the newest, finest root tips to 1 month for the larger, older roots. There were 15 unique plant-soil systems analyzed. Residual water content and field capacity of the chambers was $2.5 \text{ cm}^3 \text{ cm}^{-3}$ or ~30, respectively (ref. Kang et al., 2014) and water content during imaging ranged from ~10 to ~25 to $\text{cm}^3 \text{ cm}^{-3}$, depending on chamber. Whole chamber bulk density including the plant roots varied by chamber, ~ $1.38\text{--}1.53 \text{ g cm}^{-3}$, leading to estimated porosity ranging from 0.42 to 0.48%.

2.2. Neutron radiography conditions and experiment

Neutron radiography experiments were conducted at the CG1D beamline at the High Flux Isotope Reactor (HFIR) at Oak Ridge National Laboratory. Neutron attenuation by the plant-soil system was detected with a $25 \mu\text{m}$ LiF/ZnS scintillator linked to a charge-coupled detector (CCD) camera system (iKon – L 936 Andor Technology, Belfast, UK). The cold neutron wavelength λ ranged from 0.8 to 6 Å, with a peak neutron intensity of 2.2×10^6 at 2.6 Å. The field of view (FOV) for this experiment was $7.4 \times 7.4 \text{ cm}$, with pixel resolution of $32 \mu\text{m}$ and effective resolution $\sim 100 \mu\text{m}$ (Fig. S10). Aluminum and sand (SiO_2) have low attenuation coefficients to cold neutrons compared to water, and as such the plant-soil system enabled accurate imaging and transmission of the neutron flux. As the FOV of the beam was smaller than the individual plant containers, multiple overlapping (~5%) radiographs were taken of a single container by automatically moving the containers up, down, left and right using a motorized lift table. Exposure time for each image was 80–120 s, with consistent beamtime exposures for each experimental sample. Dynamic experiments were attempted on chambers which had sufficient resolution of roots (e.g., water content well below field capacity). For those chambers whose water content was towards the lower end of the water retention curve (Kang et al., 2014), a pulse of water was added to the surface, the volume based on their daily water use over

prior days. Irrigated water was typically allowed to redistribute for 20 min, then sequential imaging was initiated and allowed to run, typically overnight with a high-pressure sodium growth lamp (16,000 lumens) suspended overhead to drive transpiration. Temperature in the beamline was $\sim 21^\circ\text{C}$ and humidity $\sim 23\%$. A number of dynamics experiments failed due to a variety of issues (e.g., growth lamp burnout, translation stage error, data storage capacity reached). Of the successful experiments conducted, six were dynamic with sequential images collected over time as roots extracted water (five with poplar, one with maple); nine were static.

2.3. Image reconstruction and segmentation

Neutron radiographs were normalized with respect to the open beam and dark field, effectively converting them into transmission images. Open beam radiographs are exposures without samples and thus consist of only the neutron beam. Dark field radiographs are exposures with the beam turned off and thus consist of only background and detector noise. The 16 overlapping radiographs of each container were stitched together using open-access code available at the beamline (Bilheux and Bilheux, 2015; Appendix A). The code identifies identical sections of each image and overlays them into a single composite image.

We segmented all visible plant roots in the neutron image using mean-based local thresholding and morphological cleaning methods as in Dhiman et al. (2018). For each sequence of images for a single plant we selected the image when the sand was its driest to ensure the largest degree of contrast between sand and root. Then roots were identified, segmented and a root mask was created (Appendix A; Dhiman et al., 2018). The masking algorithm underestimates the very smallest fine roots (<0.01 cm) as tested using digitally scanned flatbed images of the roots. These results were expected as the finest root sizes were approaching neutron image resolution. Root were difficult to distinguish in some water-saturated sections of the images at the bottom of the containers and those sections were not used in this study.

2.4. Water content determination

We followed the methodology outlined and verified by Kang et al. (2013) to calculate volumetric water content. The water thickness of the plant-soil system was derived from the following equation:

$$\tau_w = -\frac{\Sigma_w}{2\beta} - \sqrt{-\frac{\Sigma_w}{2\beta} - \frac{1}{\beta} \ln(I_{total} - \Sigma_{Al}\tau_{Al} - \Sigma_{Si}\tau_{Si})}$$

where $\Sigma_w = 2.6844 \text{ cm}^{-1}$, $\Sigma_{Al} = 0.1089 \text{ cm}^{-1}$, and $\Sigma_{Si} = 0.2753 \text{ cm}^{-1}$ are the attenuation coefficients of water (at density 1 g cm^{-3}), aluminum (2.7 g cm^{-3}) and silica (SiO_2 ; 2.65 g cm^{-3}) at peak energy distribution (2.53 \AA), respectively; τ_w , τ_{Al} = 0.2 cm and τ_{Si} = 1 cm are the thicknesses of water, aluminum and silica, respectively; $\beta = -2.140 \text{ cm}^{-2}$ is the empirical correction factor for beam hardening and scattering effects, and I_{Total} is the corrected neutron transmission intensity (Kang et al. 2013). Water thickness was converted to per pixel volumetric water content (Fig. 1b) by dividing by sand thickness or converted to water volume by multiplying by pixel area ($32 \mu\text{m} \times 32 \mu\text{m}$).

2.5. Integrated plant-soil mapping

We identified three regions of each plant-soil system: (1) the root “skeleton” from which root diameter is derived, (2) the root surface edge and (3) the soil pixels surrounding the root and assigned to the closest root diameter segment (Fig. 2a–c). Each step is outlined below and further detailed in Appendix A.

Using the root mask as a base (highlighted in green in Fig. 2a), we first calculated local root system architecture (RSA) traits via root morphological characteristics (diameter, surface area, root order). A medial axis transform (MAT) was applied to the root mask to produce an

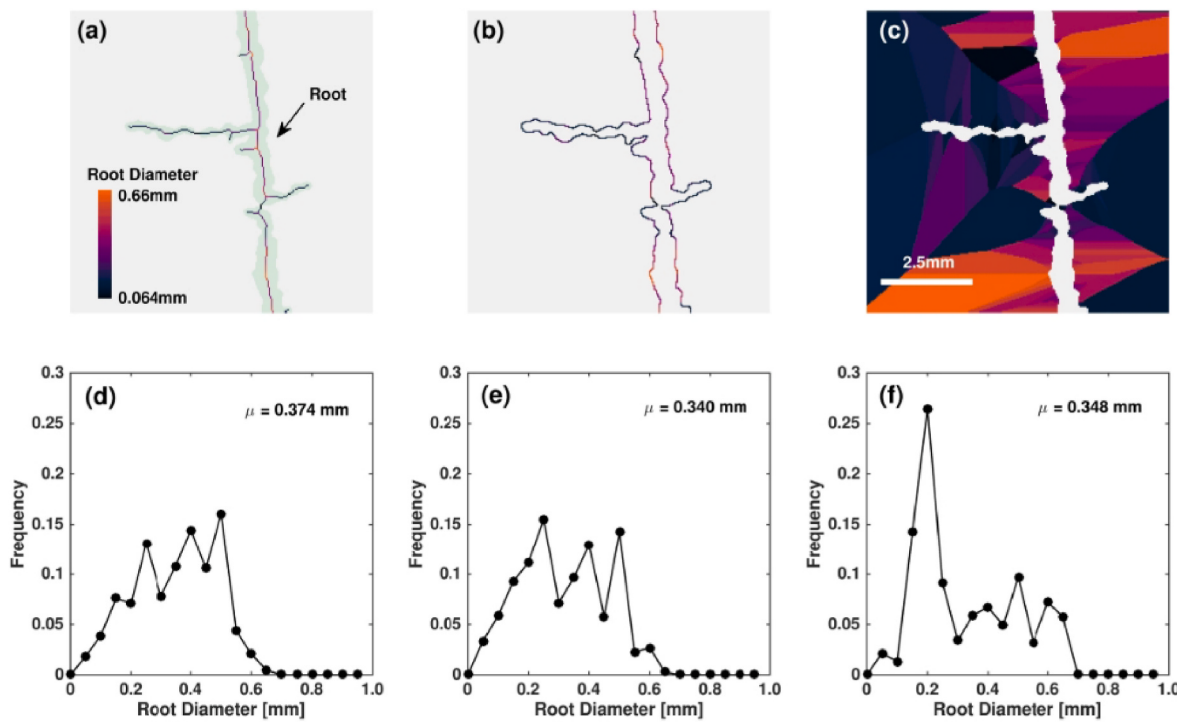


Fig. 2. Visual schematic of the plant-soil mapping procedure, and how represented root diameter classes are calculated for each transform. Using a root segment extracted from a radiograph: (a) the medial axis transform (MAT), with the root highlighted in green for reference. (b) the root surface (RS) transform. (c) the soil region (SR) transform, colors indicate root diameter, as in (a). Histograms of the represented root diameter values are shown for the (d) MAT, (b) RS and (c) SR mapping. (For interpretation of the references to color in this figure legend, the reader is referred to the Web version of this article.)

individual pixel-based topological skeleton of the root (Fig. 2a). We used this MAT to calculate root diameter – the minimum distance of each pixel to the outer edge of the root was multiplied by a factor of 2. Root surface area was calculated by multiplying diameter by π and summing skeleton pixels corresponding to a given root diameter. A key assumption made on the root morphology here is that all roots are cylindrical, and each side of the root is uniformly distributed from the medial axis. Root order analysis was conducted by manually delineating multiple regions of interest (ROIs); 226 ROIs across 5 of the 6 dynamic samples were analyzed. ROIs were selected based on visual assessment that individual root segments were isolated and not confounded due to adjacent or overlapping root sections.

As an intermediate step, a root surface map was created, defined as the 8-connected perimeter map of the root, where the calculated root diameter value in the MAT is assigned to each pixel in the root surface map based on minimum distance (Fig. 2b). Finally, we then created a watershed area map, which assigned each soil pixel to the adjacent root section based on minimum distance (Fig. 2c). Conceptually, this is like the 3D distance transforms first applied by Koebernick et al. (2014) and modeled by Schluter et al. (2018), where soil voxels were connected to dynamic RSA characteristics based on histograms of root-soil distance. However, for this analysis RSA was constrained as a static measurement. The root diameter of each root surface pixel could then be linked to distance to any given soil pixel. This allowed evaluation of soil water dynamics in context of plant root characteristics for each pixel. Note that due to RSA characteristics (e.g., root position, branching degree), the distribution of represented root diameters varies between mapping system (Fig. 2d–f); we only use the root diameter values determined in the MAT. All pixels within $\sim 1.3 \text{ cm}$ (400 pixels) from all root surfaces were evaluated. This procedure assigned a local root diameter value to every component of the plant-soil interface. After averaging across root diameter classes in each image this outputted 11,100 data points. The root processing procedure is further detailed in Appendix A and the Python-based software package is available: [https://pypi.org/project/r](https://pypi.org/project/rootprocessing/)

ootprocessing/.

2.6. Soil and rhizosphere water dynamics

We calculated radial soil water content distribution and dynamics away from the root by dividing each subsection into three classes: the rhizosphere soil ($d = 0\text{--}0.15 \text{ cm}$), which includes the root-soil edge ($d = 0\text{--}0.01 \text{ cm}$ from the root edge) and the bulk soil ($d = 0.5 \text{ cm}$) (Fig. 3). The rhizosphere zone can vary in thickness over time as roots develop and in response to environmental and edaphic conditions. The rhizosphere zone as defined here displays a much larger variation in water retention than the bulk soil (e.g., Fig. 3b, zone II), likely because of root release of mucilage (Carminati et al. 2010; Carminati, 2012; Carminati et al. 2016). All soil pixels analyzed represent purely soil values – given the 2D nature of the images, any pixel values that have a root section would be represented by both roots and soils, as soil lies in front and behind the root. Similarly, the water content of a soil pixel located 0.01 cm from the root edge would represent an integrated signal of water content through the 1 cm thickness of soil at that location and thus technically include both ‘rhizosphere’ and ‘bulk soil’ components; results should be considered in that context. This artifact can be overcome using 3D computed tomography; however, at the expense of temporal resolution (e.g., Tötzke et al. 2021). Fine roots less visible to neutron imaging (i.e., $< 100 \mu\text{m}$) also impact measured pixel saturation across the samples and thus inject additional uncertainty/variability into the analyses. As the sand was sufficiently dry, drainage was a minor factor; even so, the bottom areas of some individual chambers were too wet to image, e.g., the very bottom of the chamber shown in Fig. S9. As the top of the container was covered with tape, evaporation was a minor factor. Thus, changes in spatial and temporal patterns of water content are assumed to be dominated by local root water extraction.

The subdivision of the rhizosphere zone in this paper is a more explicitly outlined formulation of the one often used in the rhizosphere imaging literature (Fig. 3a; e.g., Carminati et al. 2010; Zarebanadkouki

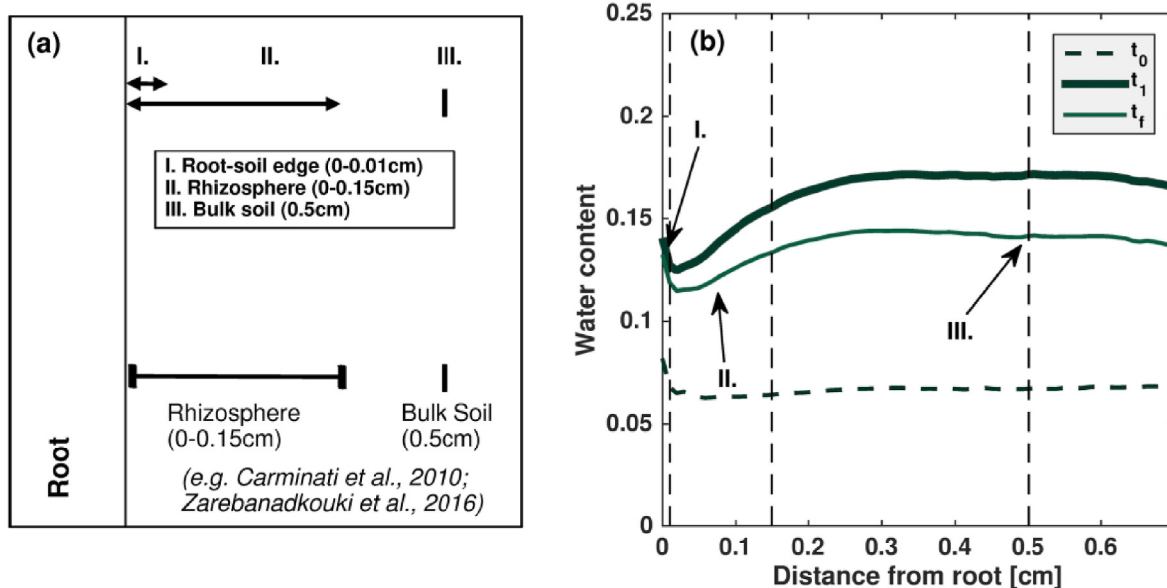


Fig. 3. (a) Outline of the three soil subsections in the plant-soil interface. (b) Outline of the location of the three soil subsections in the context of a typical water content profile in the plant-soil interface. Note the large spatial variation in hydration dynamics within the rhizosphere as compared to the bulk soil, indicating the selected rhizosphere thickness of 0.15 cm captures most of the rhizosphere thickness in this example.

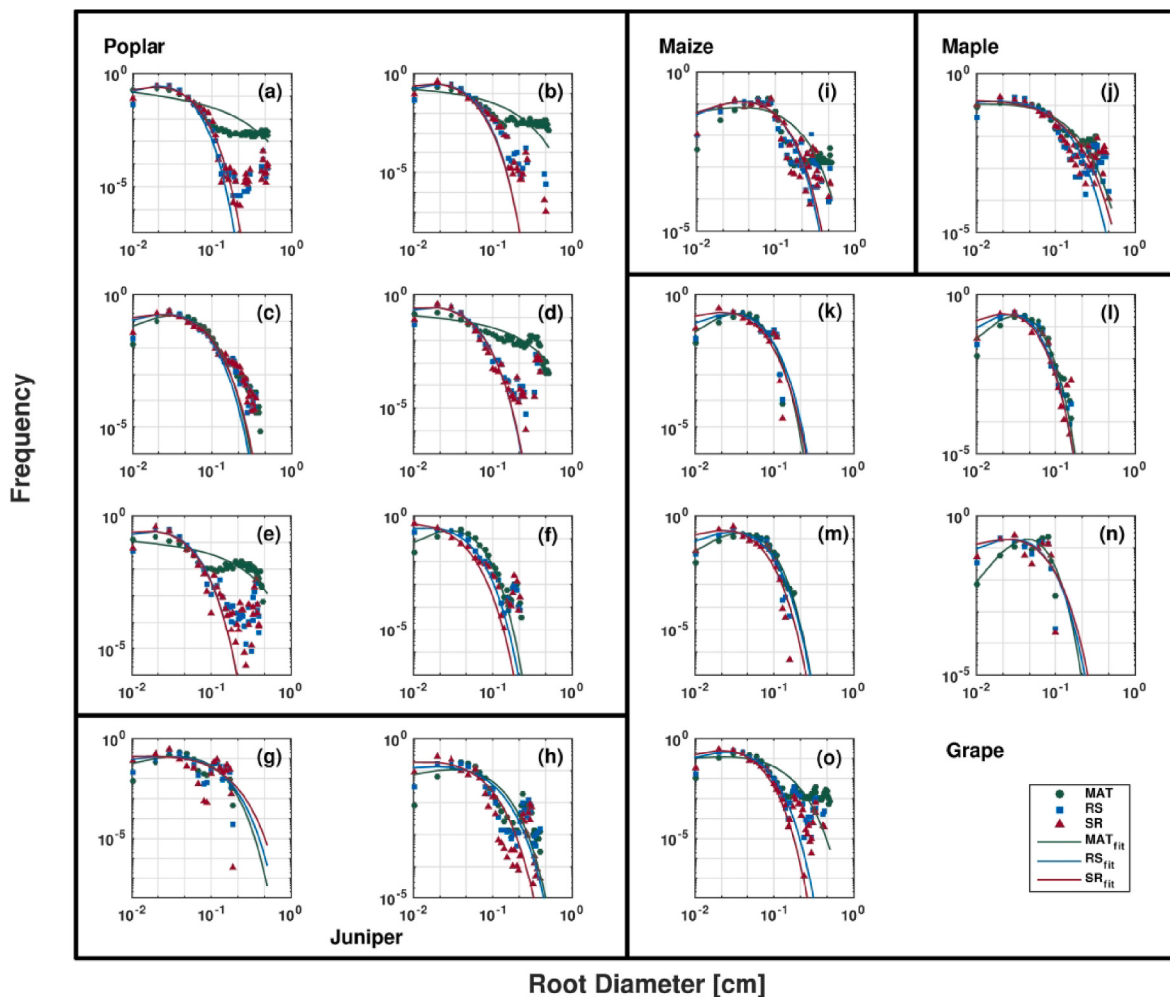


Fig. 4. Distributions of represented root diameter for the MAT, RS and SR mapping (Fig. 2) for each sample, with gamma distribution fits shown. Note axes are in log-scale.

et al. 2018). The soil region defined as the root-soil edge and the rhizosphere is often conflated and quantified interchangeably within the literature. A typical radial water content profile and how it changes with soil wetting is illustrated in Fig. 3b. For some samples where sequential neutron radiographs were collected, dynamic root water uptake was calculated by assessing the change in the volumetric water content in each specified soil subsection assigned to a root segment and summing them by root diameter over a unit of time. The data were additionally normalized to surface area by dividing the water content change by total root surface area of that given root diameter subsection, assuming a cylindrical root.

3. Results

3.1. Integrated watershed root-soil mapping

The histograms of root diameters of the integrated plant-soil map labeled as medial axis transform (MAT), the root surface (RS) and the surrounding soil region (SR) resembled gamma distributions, with most roots dominated by the fine root classes, and a long tail of thicker roots, though the fits typically underestimated the frequency of thicker root diameters (Fig. 4). The best fits to the gamma distribution were observed in the grape system (Fig. 4k, l, m), which had few thick roots. While the fine root diameter classes dominate in frequency in all samples, the RS and SR mapping show similar distributions to each other than with the MAT mapping, which shows the most deviation both from the gamma distribution fits and from the other two mapping procedures. This aspect was most notable in most of the poplar experimental samples (Fig. 4a, b, d, e) where the frequency drops almost two orders of magnitude in the thicker root diameter classes. These results are capturing the below-ground portion of the cutting (ramet) segment, and as such are an artifact. A similar pattern was also observed in one of the grape samples that had several larger roots (Fig. 4o), but the frequency drop was smaller and more scattered.

Evaluating the plant-soil system in the radial dimension, root distance histograms (RDHs) of the Euclidean distance transforms also resembled gamma distributions for all 5 species analyzed (Schluter et al. 2018), suggesting well-developed root systems – fitted parameters are shown in Table 1.

This analysis was extended to each soil region for each root diameter class to calculate the mean of each RDH, which we label mean “soil-root extent”, and which we interpret as a measure of accessible soil to a specific section of root, similar to how each area of a watershed feeds into specific sections of a stream (Fig. S5). In this analysis, the ‘watersheds’ remains independent of one another, for simplicity (discussed below). In a majority of experiments, a relatively high soil-root extent was observed for the smallest root diameters, which then show decreasing trends with increased root diameter. In half of the 15 samples (Fig. 5b, d, f-h, k, m), an uptick in soil-root extent is observed for the largest root diameters. Again, we use Fig. 2c as a visual example – the dark zones associated with the finest root diameters extend the longest in the radial direction, which would result in a high accessible soil-root extent. On the other hand, the orange zones, associated with larger root diameters, are typically “crowded out” by these blue zones, resulting in

smaller areas and thus smaller accessible soil volume to a particular root segment.

3.2. Water content distribution

Mean water content of the plant-soil system at the three soil regions of the soil for the 6 experimental samples (5 poplar, 1 maple) with dynamic imaging through time are shown in Fig. 6. Water content dynamics varied with drying or wetting regimes: under dry conditions (water withheld for one or more days), water content at the root-soil edge was greatest amongst the three classes and had the greatest difference between it and the other two soil regions. Following rewetting, this difference decreased, and in the case of one poplar experiment (Fig. 6e), the bulk soil and rhizosphere water content increased above that of the root-soil edge, though subsequent water content decrease in the latter was minimal compared to the former two regions. While water content distribution was heterogeneous across and within species samples, we observed that inter- and intra-species generalizations can be more readily made when comparing relative differences in water content across the three analyzed soil subsections.

We highlight these variable differences in water content distribution across all six species in Fig. 7, where we take the mean water content of the three soil subsections and calculate the difference in water content at the two interfaces between them, for each root diameter class in a single image. Data shown here correspond to the driest image of each experimental sample, including the initial pre-wetting image of the dynamics experiments. We observe that root-soil edge/rhizosphere water content difference is low for the finest root diameters – this difference increases steadily until a root diameter of roughly 0.12–0.20 cm – beyond this point we observe the water content difference stabilize to ~0.1. Similar relationships are exhibited when assessing by individual genus (Fig. S11). Given the nature of the distribution, we fit the data with a sigmoid function, with the following fitting parameters:

$$\Delta\theta = \frac{L}{1 + e^{-k(D_{root} - x_0)}}$$

Where $\Delta\theta$ is the water content difference between the two soil subsections, L is the maximum water content difference, x_0 is the root diameter midpoint of the curve, and k is the steepness of the curve. Best fit values corresponding to the function are shown in Table 2.

We observe similar distributions across all five species analyzed. In contrast, there was no relationship in water content difference between the rhizosphere and bulk soil across diameter during the driest period (Fig. 7b). Water content differences at the root-soil edge/rhizosphere interface were almost always >0, but water content differences at the rhizosphere/bulk soil interface regularly exhibited both negative and positive values indicating wetter or drier rhizosphere soil as compared to bulk soil.

We then extend this analysis of relative change in water content across the entire soil moisture range in Fig. 8, where we plot mean water content difference in the root-soil edge/rhizosphere interface (top row), and in the rhizosphere/bulk soil interface (bottom row), by root diameter class. Given its organizational structure, a plot can be divided into quadrants: using Fig. 8d as an example - the zones above and below the dotted line indicate wetter or drier rhizosphere soil relative to bulk soil, while the left and right zones indicate respectively drier or wetter soil water regimes. The edge-rhizosphere interface relationship highlights what was observed in Fig. 7a – all points are greater than 0 regardless of root diameter, indicating the root edge water content is equal to or wetter than the rhizosphere soil regardless of bulk water soil water content. The increased difference in root edge to rhizosphere water content with root diameter is observed as well (Fig. 8a–c). Very few data points are below the reference zero line, and given the shallow slope of the data, the linear fit never crosses the reference line. In contrast, across the rhizosphere-bulk soil interface, the rhizosphere water content is

Table 1

Gamma distribution parameters of the root distance histograms of each species evaluated in our experiments. Columns 1 and 2 represent mean parameters k and Θ across all samples for a given species, and columns 3 and 4 represent the mean and variance of the gamma distributions.

	k	Θ [cm]	mean [cm]	var [cm^2]
Poplar	0.8029	0.63454	0.50947217	0.32328047
Maple	0.8941	2.09375	1.87202188	3.9195458
Grape	1.1918	0.54502	0.64955484	0.35402038
Juniper	1.1887	0.71732	0.85267828	0.61164319
Maize	0.8698	0.377	0.3279146	0.1236238

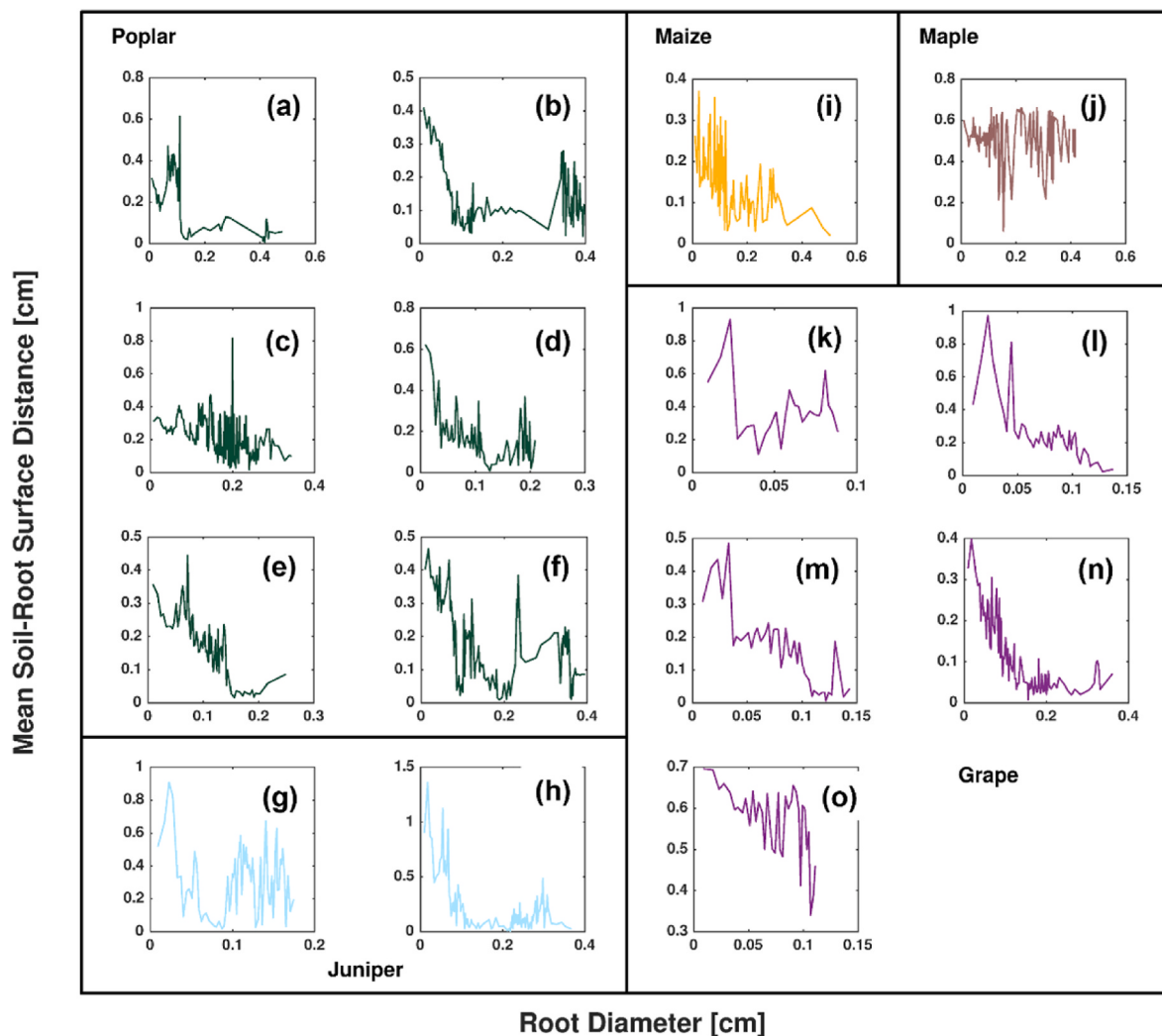


Fig. 5. Mean plant-soil extent of all soil pixels to the closest root surface, sorted by root diameter. (a–f) poplar, (g, h) juniper, (i) maize, (j) maple and (k–o) grape experiments.

wetter than the bulk soil under drier conditions, but drier than the bulk soil under moister conditions (Fig. 8d–f). This relationship is independent of root diameter. The average transition point between a wetter or drier rhizosphere for this sand was 0.11, 0.10 and 0.13 $\text{cm}^3 \text{cm}^{-3}$ for the small, medium and large root diameter classes, respectively; however, the spread in the data indicate substantial variability. When classified by root order, these trends are considerably less pronounced (Fig. 9), although there is a similar transition point between rhizosphere and bulk soil water content (Fig. 9e–h) at $\sim 0.10 \text{ cm}^3 \text{cm}^{-3}$ and a root-soil edge water content slightly higher than the rhizosphere water content (Fig. 9a–d) across the full bulk water content range.

3.3. Water uptake

In the dynamic samples there was a non-linear decline in apparent water uptake with increased root diameter (Fig. 10a). Apparent water uptake is based on water depletion around specific roots, but there could be a depletion near an inactive root due to movement of that water towards an active root. This confounding root uptake and soil water transport pattern would be most prevalent in wetter soils. In addition, roots with greater uptake rates create a gradient in water content away from the root. Thus, an improvement to our technique would be to quantify this gradient in water content change over time around all roots, allowing for competition between roots, in this case, competition

between the root ‘watersheds’. While much more complex at the pore level, these data could be used to test Richard’s type models of pore-scale water movement across an entire root system. The smallest root diameter classes ($<0.05 \text{ cm}$) exhibited a similar magnitude of water uptake per unit surface area across species, with rates declining by 1–2 orders of magnitude with root diameter until $\sim 0.1 \text{ cm}$. Water uptake rates were variable for larger roots and maple had greater uptake rates than poplar. However, in both species, normalized water uptake rates continued to decline with increased root diameter.

Across all samples analyzed, total root surface area of the finest roots were orders of magnitude greater than that of the larger root diameter classes (Fig. 10b). When evaluating total water uptake by the plant root system for the 6 dynamics experimental samples, we see a strong linear correlation with total calculated surface root area (Fig. 10c).

4. Discussion

4.1. Integrated plant-soil mapping

The three-tiered plant-soil mapping procedure outlined in our paper emphasizes the morphological consequence of root system size and distribution on the surrounding soil system, in this case a fine quartz sand. The proportionally higher representation of the fine root classes in the root surface (RS) and the surrounding soil region (SR) mappings are

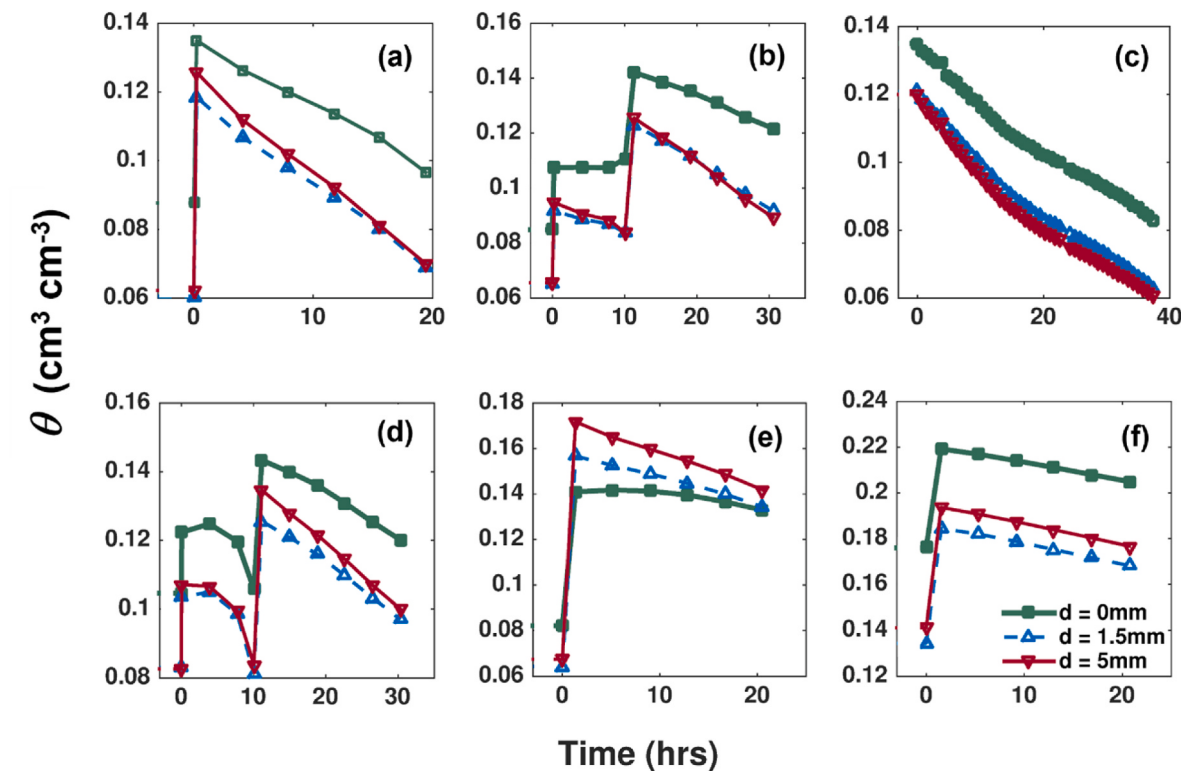


Fig. 6. Mean water content (θ) over time for the three soil region boundaries based on distance from root edge, 'd', in the root-soil interface for the (a-e) poplar and (f) maple systems. Following initial imaging at time 0, all containers were irrigated, except panel c. A second re-wetting event occurred at 10 h for panels b, d.

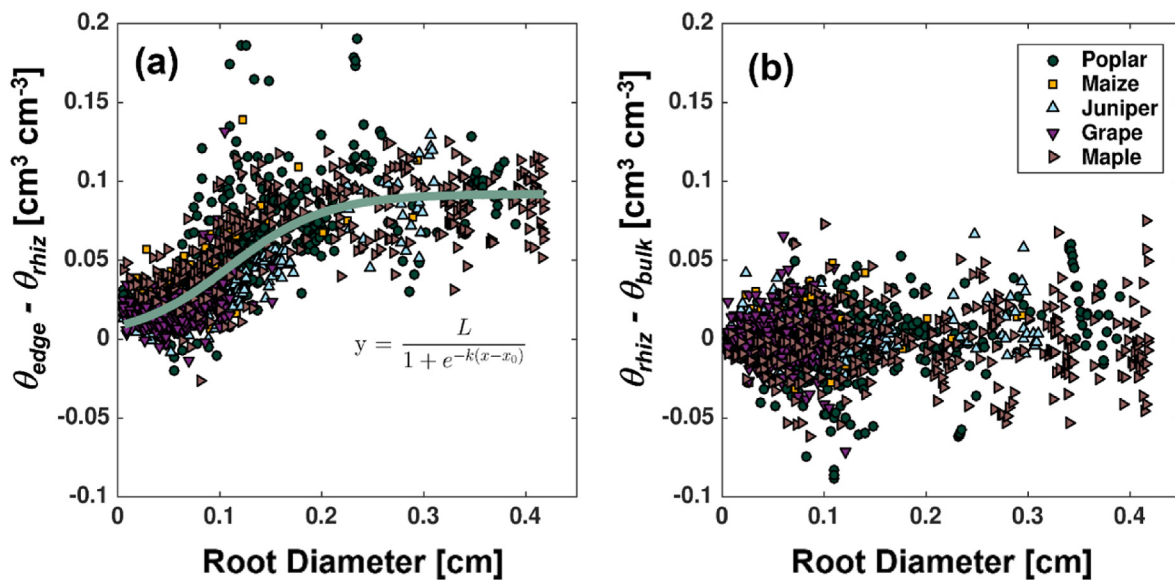


Fig. 7. (a) Difference in water content ($\text{cm}^3 \text{cm}^{-3}$) between the root-soil edge and the rhizosphere sorted by root diameter for multiple species growing in sand. Data were collected at the driest point for each root system. The best fit sigmoid regression is indicated by the green line. (b) difference in water content between the rhizosphere and the bulk soil, sorted by root diameter. (For interpretation of the references to color in this figure legend, the reader is referred to the Web version of this article.)

simply by virtue of the root morphological distribution and its spatial distribution in the soil. In one example, a root tip, often the smallest portion of the root, will have access to more soil regions, simply by virtue of being at the end of the root (although the root tip itself cannot take up much water, the section behind it can). Another example is that the finest root diameter classes often induce a root crowding effect, where the smaller roots (and their associated zones) surround

intermediate-sized roots, which means that less soil is exclusively assigned to the latter. The root tip effect is visible in Fig. 2c, which subsequently crowds and minimizes the surrounding thicker root soil regions. Similar spatial crowding and access to soil zones and soil water has been described for barley root hairs (Segal et al., 2008).

While a straightforward metric to use for our integrated plant-soil mapping, some constraints apply regarding our implementation of

Table 2

Best fit parameters and root mean square error of the sigmoid functions fitted for the five species analyzed in Fig. 7a (ref. Fig. S11), as well as the combined data.

Species	L [$\text{cm}^3 \text{cm}^{-3}$]	k	x_0 [cm]	RMSE
Combined	0.092	21.1	0.11	0.0185
Poplar	0.0943	23	0.103	0.0199
Maize	0.113	11.6	0.128	0.0179
Juniper	0.11	15.3	0.175	0.0109
Grape	0.147	14.7	0.191	0.011
Maple	0.0887	20.3	0.0764	0.0196

spatial proximity as the sole criteria considered for connecting plant and soil characteristics. While root water uptake influence can extend to the cm-range and further (Darrah, 1993), some root morphological classes may not have this capability, and thus should be excluded during the matching process of the root-soil mapping. With regards to the root crowding effect, it is unlikely that only a single root diameter or root surface has exclusive influence on all soil characteristics in that pixel, especially for processes like water uptake. Creating an additive component, where soil pixels can have variable degrees of root morphological assigned value as weighted by spatial proximity, root diameter and root developmental stage would be useful for analysis of more detailed uptake kinetics.

4.2. Rhizosphere distribution and dynamics

In our general analysis of the rhizosphere, we classified two key interfaces: the edge-rhizosphere interface and the rhizosphere-bulk soil interface. Water content differences across these interfaces serve as a simple metric for rhizosphere development, as larger differences in water content and retention between adjacent soil likely indicate more

deviations from unaffected soil (e.g., Carminati et al. 2010). Using this interpretation, our results suggest that rhizosphere development is consistently pronounced at the edge-rhizosphere interface under the full soil moisture range (Fig. 8a–c) and shows a sigmoidal relationship with root system architecture (RSA) development (i.e., increasing root diameter, Fig. 7a). In contrast, rhizosphere development displays hydraulic plasticity that is dependent on local bulk soil moisture content (Fig. 8d–f), and no discernible influence from RSA properties (Fig. 7b). Of note, we observe this phenomenon across all five plant species analyzed, despite observed differences in RSA spatial distribution and root morphological traits.

How do we explain these different trends observed at each of the rhizosphere interfaces? For the edge-rhizosphere interface, a potential driving factor is root release of mucilage (a polymeric gel shown to be active in younger, thinner roots; Ahmed et al. 2014) or other exudates. Significant concentrations are typically seen 0.005–0.01 cm from the root surface (Oades 1978; Foster, 1988; Carminati et al. 2015). This corresponds to the dimensions of our root-soil edge, which we make explicit in addition to the remaining rhizosphere, typically demarcated between 0 and 0.15 cm in prior studies (Carminati et al. 2010), although this rhizosphere zone is dynamic due to root age, morphology and interactions with soil physical, chemical and biological characteristics. Along with root hair presence, root exudates can increase water retention across water potentials (Carminati et al. 2016), which can explain the consistently higher water contents in the rhizosphere. For the rhizosphere-bulk soil interface, bulk soil characteristics may be more dominant factor controlling water retention than root released compounds, given the consistent transition point independent of root morphology or species. The calculated transition water content (when the rhizosphere changes from wetter to drier than other zones, Figs. 8 and 9, $\sim 0.11 \text{ cm}^3 \text{cm}^{-3}$) corresponds to a matric potential of $\sim 2 \text{ kPa}$

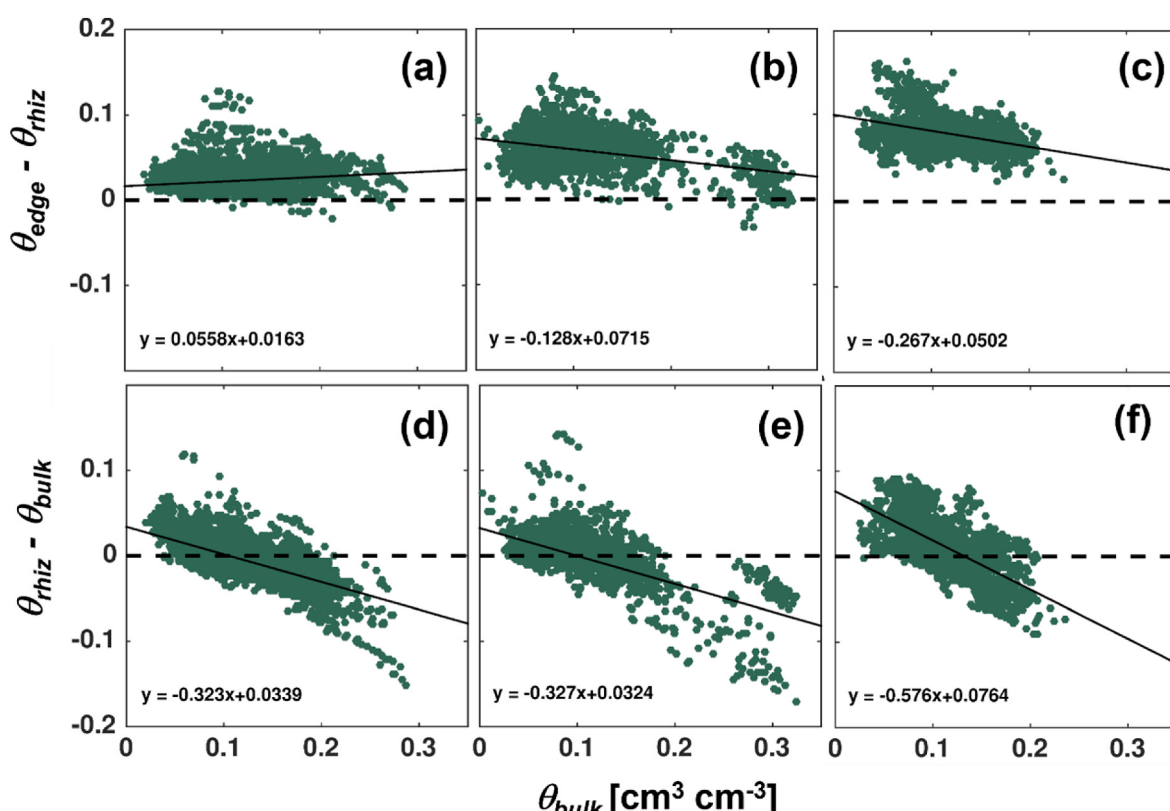


Fig. 8. Relative water content dynamics, as sorted by root diameter. (a–c) Difference in water content ($\text{cm}^3 \text{cm}^{-3}$) from root-soil edge to rhizosphere versus bulk soil water content, for root diameters (D_{root}) (a) $< 0.1 \text{ cm}$, (b) $0.1\text{--}0.2 \text{ cm}$, and (c) $> 0.2 \text{ cm}$. (d–f) Difference in water content ($\text{cm}^3 \text{cm}^{-3}$) from rhizosphere to bulk soil versus bulk soil water content, for root diameters (d) $< 0.1 \text{ cm}$, (e) $0.1\text{--}0.2 \text{ cm}$, and (f) $> 0.2 \text{ cm}$. Dotted lines show reference line where soil subsections at either side of the interface are equal; solid lines are best linear fits.

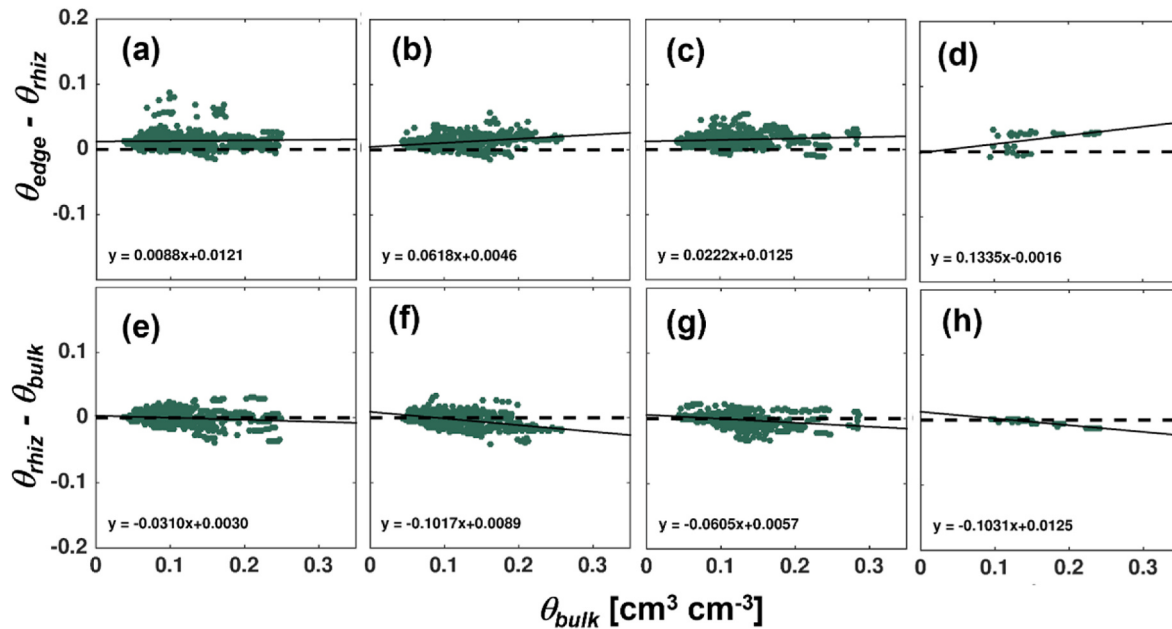


Fig. 9. Relative water content dynamics as sorted by root order. Difference in water content (cm³ cm⁻³) from root-soil edge to rhizosphere versus bulk soil water content, for (a) 1st, (b) 2nd, (c) 3rd, and (d) 4th root orders. (e-h) Difference in water content (cm³ cm⁻³) from rhizosphere to bulk soil versus bulk soil water content, for (e) 1st, (f) 2nd, (g) 3rd, and (h) 4th root order. Dotted lines show reference line where soil subsections at either side of the interface are equal; solid lines are best linear fits.

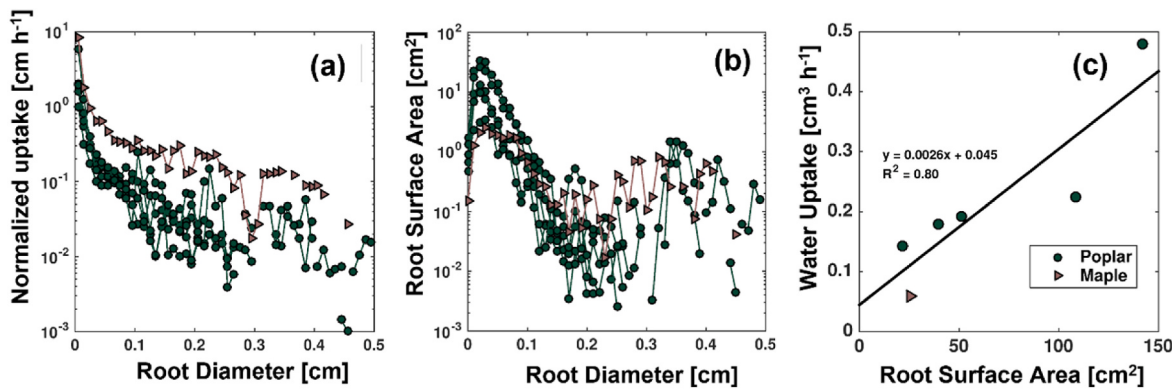


Fig. 10. (a) Total water uptake normalized by total root surface area across root diameters, (b) distribution of total root surface area by root diameter, (c) total root water uptake of all dynamics experimental samples plotted by total root surface area.

based on the Brooks and Corey soil water retention parameters calculated for this sand (Cheng et al. 2012; Kang et al. 2014). While a relatively low matric potential, this point is situated at the lower end of the water retention curve for this sand. At soil water potential values lower than this the water availability drops exponentially, quickly approaching residual water content. The fact that edge-rhizosphere interface values are changing with root morphological traits, while rhizosphere-bulk soil interface values are independent of these parameters highlights the multiple processes at play within a single rhizosphere, and the need to clarify appropriate boundary conditions for each edge of the rhizosphere. Transplanting, and the use of pure sand in this study does control to an extent root morphology (including root hairs, growth patterns, associations with mycorrhizal hyphae), rhizosphere development and soil hydraulic characteristics. Clay, loam or organic soils that are more common in nature would each have their own distinct characteristics, and results should be considered in that context.

Although at a much lower magnitude, sorting by root order shows

similar trends in root-edge, rhizosphere and bulk soil water dynamics. This is somewhat contrary to the literature, which has shown non-uniform exudate deposition along the lateral dimension of the root by species (e.g., Razavi et al. 2016) and switching of water uptake location by root order as root size increases and matures (Ahmed et al. 2018b; Dhiman et al., 2018). This may be due to species differences (maize vs. maple/poplar) that vary in root traits (e.g., architecture, diameter vs order, symbionts), or perhaps our limited manual sampling. Another aspect may be that our root diameter distribution within the root-order ROIs analyzed fall under a narrower range of root diameters (<0.1 cm) that are all highly functional in these young plants and furthermore approach the diameter range on the order of ~0.01 cm that our segmentation procedure has shown to underestimate (Dhiman et al. 2018), leading to lower root lengths for this diameter class. These two aspects limit the extent our ability to link uptake kinetics to root order; however, future work that leverages advances in neutron detectors and imaging techniques may resolve order-based uptake rates *in situ*. Another

promising metric is using normal species-specific distribution intervals of root diameter as an effective proxy for root order (e.g., Liu et al. 2018), which could work well with our plant-soil mapping procedure.

The strong decline in apparent water uptake rates with increasing root size seen in this study is consistent with earlier work. Water uptake is high in the early stages of root development as the root tissue develops but decreases as they mature or begin to senesce (Wells and Eissenstat, 2003). Radial conductivity of water into the root varies with distance from root tip, with an estimate 90% of total water uptake conducted by just 30% of the root surface (Zwieniecki et al. 2003). The most distal root tips that are smallest in diameter have less developed xylem vasculature and take up less water than the root sections some distance back from the tip (Zwieniecki et al. 2003; Ahmed et al. 2016a). As roots age the process of suberization of endodermal cells limits uptake as roots transition to more transportive roles. Younger, smaller roots are more permeable to water (Dhiman et al. 2018) and combined with potential suberization of the larger root classes, this may explain the large difference in water uptake we see here. Another potential explanation is differences in mean soil-root extent – in 5 of the 6 poplar experiments, the finest root classes have the largest soil-root extents. While this means that water must travel a further distance through the sand to reach the location of root uptake, it also means that more water overall is available to that given root class driven by saturated or unsaturated flow into the localized depletion zone. Root water availability was controlled to some degree due to the 1.3 cm (400 pixel) boundary applied, though this does not change the fact that the peripheral roots have preferential access to soil water on the outer edges of the RSA. This may contribute to greater total water uptake in the fine roots just by virtue of physical proximity to the soil (less competition for soil water), or over time by root growth into more saturated soil. The soil-root distance for maple was relatively consistent across root diameter, which may explain the lower magnitude decrease in normalized water uptake with root diameter compared to other species. An important point to note is that the youngest, smallest roots in our experiments are underestimated due to resolution and segmentation limitations (Dhiman et al. 2018). Full inclusion of these very fine roots would increase their root surface area and thus would decrease water uptake per unit surface area in the smallest root classes, though their total water uptake remains unchanged. Presence of extra-radical mycorrhizal hyphae would further confound both rhizosphere water content and root water uptake due to their impacts on soil water retention curve parameters (e.g., Marcacci et al. 2022) or via hyphal water uptake and transport to the root (e.g., Read and Boyd, 1986). In addition, hydraulic redistribution by roots (Caldwell and Richards, 1989; Hayat et al., 2020) or mycorrhizal hyphae (e.g., Egerton-Warburton et al., 2008; Warren et al. 2008; 2013) further confound patterns of soil rhizosphere water content and uptake.

4.3. Incorporation of dynamic processes

In our study, individual plants were directly transplanted with a developed root system, so all rhizosphere development in the sand commenced simultaneously in an individual sample, allowing us to evaluate coupled root-soil properties more directly. Incorporating a dynamic element to the spatial range of the rhizosphere (as opposed to the static 0.15 cm distance used here and elsewhere, e.g., Carminati et al. 2010; Zarebanadkouki et al. 2016) may be necessary if evaluating differential shifts in root diameter and morphology over time.

Root tips not only produce mucilage but also shed root cells into the rhizosphere due to abrasion and soil structural resistance (Groleau-Renaud et al. 1998; Read et al. 2003). Mucilage, exudates, root tissue litter and root turnover all have an effect on rhizosphere development for the rest of the root that develops within the same trajectory. In this regard, incorporating dynamic RSA would provide a more complete picture of rhizosphere development across the full root system growth range. In our study, we used static integrated plant-soil maps, as our focus was characterizing short-term soil and root water dynamics. Root

growth was minimal for the duration of our experiments, as the experiment RSAs were already developed and maximum duration of experiments was approximately 40 h. Changing this to a dynamic mapping system over time would provide a more comprehensive analysis of rhizosphere development in the context of evolving plant and soil characteristics. Given its sensitivity to water, neutron imaging is invaluable in characterizing soil water dynamics of the plant-soil interface, although there are limits to the level of detail 2D radiography can provide. Recent advances in ultra-fast neutron tomography (Tötze et al. 2017, 2021) and data processing such as machine learning techniques (e.g., Venkatakrishnan et al., 2021) offer new avenues for analysis and insight. Another promising multimodal imaging method for this integrated plant-soil mapping is to leverage X-ray tomography which has been utilized to characterize pedological features of the rhizosphere (e.g., Koebernick et al. 2017), although plant damage can occur with this ionizing radiation that limits its repeated use over time. While soil or root water quantification with X-ray imaging is challenging (e.g., Moradi et al., 2009), other soil parameters (e.g., porosity, particle size distribution) can be evaluated at a pixel-by-pixel basis in conjunction with root morphological parameters.

In conclusion, our present study outlines an integrated analysis of rhizosphere characteristics by incorporating local effects of differential root morphology and bulk soil (sand) and water characteristics. By conducting this analysis on five different species across a wide range of soil moisture regimes using neutron radiography, we described a generalized, species-independent framework of rhizosphere behavior. By characterizing the plant-soil region into three domains (root-soil edge, rhizosphere, bulk soil), we calculated relative water content differences between them and evaluated them in the context of differential root diameter. We observed a consistently higher water content at the root-soil edge, which increased with root diameter, likely due to fine root release of water, exudates, mucilage and tissue. At the rhizosphere-bulk soil interface, we observed rhizosphere water content plasticity, dependent on local bulk soil water content and independent of root morphological traits – this was likely due to the characteristics of the quartz sand. Further studies with more organic or clay soils, older plant systems and with specific or native bacterial and fungal microbiomes are warranted.

Notice

This manuscript has been authored by UT-Battelle, LLC under Contract No. DE-AC05-00OR22725 with the US Department of Energy. The United States Government retains and the publisher, by accepting the article for publication, acknowledges that the United States Government retains a non-exclusive, paid-up, irrevocable, world-wide license to publish or reproduce the published form of this manuscript, or allow others to do so, for United States Government purposes. The Department of Energy will provide public access to these results of federally sponsored research in accordance with the DOE Public Access Plan (<http://energy.gov/downloads/doe-public-access-plan>).

Author contributions

JMW and HB designed the experimental setup, performed experiments and collected the data. KFD, JMW, and KC analyzed and interpreted the data. KFD and JCB developed the automated software analysis. KFD drafted the initial manuscript and JMW developed the final version, with all authors providing revision and comments.

Funding

This material is based upon work supported by the U.S. Department of Energy's (DOE), Office of Science, Office of Biological and Environmental Research (BER) Program and by Office of Science, Office of Workforce Development for Teachers and Scientists, Office of Science

Graduate Student Research (SCGSR) program. The SCGSR program is administered by the Oak Ridge Institute for Science and Education (ORISE) for the DOE. ORISE is managed by ORAU under contract number DE-AC05-06OR23100. Oak Ridge National Lab (ORNL) is managed by UT-Battelle, LLC, for the DOE under contract DE-AC05-00OR22725. This research used resources at the High Flux Isotope Reactor, a DOE Office of Science User Facility operated by ORNL.

Declaration of competing interest

The authors declare that they have no known competing financial interests or personal relationships that could have appeared to influence the work reported in this paper.

Data availability

Data will be made available on request.

Acknowledgements

We thank Joanne Childs, Steve Childs, Deanne Brice, Cari Ficken, Sara Jawdy and Mindy Clark for plant material and propagation, Shafer Powell for image analysis and Lou Santodonato for help with the CG1D beamline. We appreciate the thoughtful and detailed comments from external reviewers that improved the manuscript.

Appendix A. Supplementary data

Supplementary data to this article can be found online at <https://doi.org/10.1016/j.rhisph.2023.100738>.

References

- Ahmed, M.A., Kroener, E., Holz, M., Zarebanadkouki, M., Carminati, A., 2014. Mucilage exudation facilitates root water uptake in dry soils. *Funct. Plant Biol.* 41, 1129–1137.
- Ahmed, M.A., Zarebanadkouki, M., Kaestner, A., Carminati, A., 2016a. Measurements of water uptake of maize roots: the key function of lateral roots. *Plant Soil* 398, 59–77.
- Ahmed, M.A., Kroener, E., Benard, P., Zarebanadkouki, M., Kaestner, A., Carminati, A., 2016b. Drying of mucilage causes water repellency in the rhizosphere of maize: measurements and modelling. *Plant Soil* 407, 161–171.
- Ahmed, M.A., Passioura, J., Carminati, A., 2018a. Hydraulic processes in roots and the rhizosphere pertinent to increasing yield of water-limited grain crops: a critical review. *J. Exp. Bot.* 69 (13), 3255–3265.
- Ahmed, M.A., Zarebanadkouki, M., Meunier, F., Javaux, M., Kaestner, A., Carminati, A., 2018b. Root type matters: measurement of water uptake by seminal, crown, and lateral roots in maize. *J. Exp. Bot.* 69 (5), 1199–1206.
- Aravena, J.E., Berli, M., Ruiz, S., Suarez, F., Ghezzehei, T.A., Tyler, S.W., 2014. Quantifying coupled deformation and water flow in the rhizosphere using X-ray microtomography and numerical simulations. *Plant Soil* 376, 95–110.
- Bilheux, J-C., Bilheux, H., 2015. iMARS (iMaging Analysis Research Software). *Phys. Proc.* 69, 343–348.
- Cai, G., Tötzke, C., Kaestner, A., Ahmed, M.A., 2022. Quantification of root water uptake and redistribution using neutron imaging: a review and future directions. *Plant J.* 111, 348–359.
- Caldwell, M.M., Richards, J.H., 1989. Hydraulic lift – water efflux from upper roots improves effectiveness of water uptake by deep roots. *Oecologia* 79, 1–5.
- Canarini, A., Kaiser, C., Merchant, A., Richter, A., Wanek, W., 2019. Root exudation of primary metabolites: mechanisms and their roles in plant responses to environmental stimuli. *Front. Plant Sci.* 10 (157), 1–19.
- Carminati, A., Vetterlein, D., Vogel, H.-J., Oswald, S.E., 2009. When roots lose contact. *Vadose Zone J.* 8 (3), 805–809.
- Carminati, A., Moradi, A.B., Vetterlein, D., Vontobel, P., Lehmann, E., Weller, E., Vogel, H.-J., Oswald, S.E., 2010. Dynamics of soil water content in the rhizosphere. *Plant Soil* 332, 163–176.
- Carminati, A., Schneider, C.L., Moradi, A.B., Zarebanadkouki, M., Vetterlein, D., Vogel, H.-J., Hildebrandt, A., Weller, U., Schuler, L., Oswald, S.E., 2011. How the rhizosphere may favor water availability to roots. *Vadose Zone J.* 10, 988–998.
- Carminati, A., 2012. A Model of Root Water Uptake Coupled with Rhizosphere Dynamics. *Vadose Zone J.* 11 vzj2011.0106.
- Carminati, A., Vetterlein, D., 2013. Plasticity of rhizosphere hydraulic properties as a key for efficient utilization of scarce resources. *Ann. Bot.* 112, 277–290.
- Carminati, A., Kroener, E., Ahmed, M.A., Zarebanadkouki, M., Holz, M., Ghezzehei, T., 2015. Water for carbon, carbon for water. *Vadose Zone J.* 15 (2), 1–10.
- Carminati, A., Zarebanadkouki, M., Kroener, E., Ahmed, M.A., Holz, M., 2016. Biophysical rhizosphere processes affecting root water uptake. *Ann. Bot.* 118, 561–571.
- Cheng, C.L., Kang, M., Perfect, E., Voisin, S., Horita, J., Bilheux, H.Z., Warren, J.M., Jacobson, D.L., Hussey, D.S., 2012. Average soil water retention curves measured by neutron radiography. *Soil Sci. Soc. Am. J.* 76, 1184–1191.
- Daly, K.R., Tracy, S.R., Crout, N.M.J., Mairhofer, S., Pridmore, T.P., Mooney, S.J., Roose, T., 2018. Quantification of root water uptake in soil using X-ray computed tomography and image-based modelling. *Plant Cell Environ.* 41, 121–133.
- Darrah, P.R., 1993. The rhizosphere and plant nutrition: a quantitative approach. *Plant Soil* 155/156, 1–20.
- Dexter, A.R., 1987. Compression of soil around roots. *Plant Soil* 97, 401–406.
- Dhiman, I., Bilheux, H., DeCarlo, K., Painter, S.L., Santodonato, L., Warren, J.M., 2018. Quantifying root water extraction after drought recovery using sub-mm *in situ* empirical data. *Plant Soil* 424, 73–89.
- Egerton-Warburton, L.M., Querejeta, J.I., Allen, M.F., 2008. Efflux of hydraulically lifted water from mycorrhizal fungal hyphae during imposed drought. *Plant Signal. Behav.* 3, 68–71.
- Feeley, D.S., Crawford, J.W., Daniell, T., Hallett, P.D., Naoise, Nunan, Ritz, K., Rivers, M., Young, I.M., 2006. Three-dimensional microorganization of the soil-root-microbe system. *Microb. Ecol.* 52, 151–158.
- Foster, R.C., 1988. Microenvironment of soil microorganisms. *Biol. Fertil. Soils* 6, 189–203.
- Garrigues, E., Doussan, C., Pierret, A., 2006. Water uptake by plant roots: I. formation and propagation of a water extraction front in mature root systems as evidenced by 2D light transmission imaging. *Plant Soil* 283, 83–98.
- Gregory, P.J., 2006. Roots, rhizosphere, and soil: the route to a better understanding of soil science? *Eur. J. Soil Sci.* 57, 2–12.
- Gregory, P.J., Hinsinger, P., 1999. New approaches to studying chemical and physical changes in the rhizosphere: an overview. *Plant Soil* 211, 1–9.
- Groleau-Renaud, V., Plantureux, S., Guckert, A., 1998. Influence of plant morphology on root exudation of maize subjected to mechanical impedance in hydroponic conditions. *Plant Soil* 201, 231–239.
- Hallett, P.D., Gordon, D.C., Bengough, A.G., 2003. Plant influence on rhizosphere hydraulic properties: direct measurements using a miniaturized infiltrometer. *New Phytol.* 157, 597–603.
- Hartmann, A., Rothbäcker, M., Schmid, M., 2008. Lorenz Hiltner, a pioneer in rhizosphere microbial ecology and soil bacteriology research. *Plant Soil* 312, 7–14.
- Hayat, F., Zarebanadkouki, M., Ahmed, M.A., Buecherl, T., Carminati, A., 2020. Quantification of hydraulic redistribution in maize roots using neutron radiography. *Vadose Zone J.* 19, e20084.
- Hiltner, L., 1904. Über neuere Erfahrungen und Probleme auf dem Gebiete der Bodenbakteriologie unter besonderer Berücksichtigung der Grundung und Brache. *Arb. DLG* 98, 59–78.
- Hinsinger, P., Bengough, A.G., Vetterlein, D., Young, I.M., 2009. Rhizosphere: biophysics, biogeochemistry and ecological relevance. *Plant Soil* 321 (1–2), 117–152.
- Kang, M., Bilheux, H.Z., Voisin, S., Cheng, C., Perfect, E., Horita, J., Warren, J.M., 2013. Water calibration measurements for neutron radiography: application to water content quantification in porous media. *Nucl. Instrum. Methods Phys. Res., Sect. A* 708, 24–31.
- Kang, M., Perfect, E., Cheng, C.L., Bilheux, H.Z., Lee, J., Horita, J., Warren, J.M., 2014. Multiple pixel-scale soil water retention curves quantified by neutron radiography. *Adv. Water Resour.* 65, 1–8.
- Koebernick, N., Weller, U., Huber, K., Schlüter, S., Vogel, H.J., Jahn, R., Vereeken, H., Vetterlein, D., 2014. *In situ* visualization and quantification of three-dimensional root system architecture and growth using X-ray computed tomography. *Vadose Zone J.* 13 (8).
- Koebernick, N., Daly, K.R., Keyes, S.D., George, T.S., Brown, L.K., Raffan, A., Cooper, L.J., Naveed, M., Bengough, A.G., Sinclair, I., Hallett, P.D., Roose, T., 2017. High-resolution synchrotron imaging shows that root hairs influence rhizosphere soil structure formation. *New Phytol.* 216, 124–135.
- Liu, Y., Wang, G., Yu, K., Li, P., Xiao, L., Liu, G., 2018. A new method to optimize root order classification based on the diameter interval of fine root. *Sci. Rep.* 8, 2960.
- MacFall, J.S., Johnson, G.A., Kramer, P.J., 1990. Observation of a water-depletion region surrounding loblolly pine roots by magnetic resonance imaging. *Proc. Natl. Acad. Sci. USA* 87, 1203–1207.
- Marcacci, K.M., Warren, J.M., Perfect, E., Labbe, J.J., 2022. Influence of living grass roots and endophytic fungal hyphae on soil hydraulic properties. *Rhizosphere* 22 (100510), 1–13.
- McCormack, M.L., Dickie, I.A., Eissenstat, D.M., Fahey, T.J., Fernandez, C.W., Guo, D., Helmsaari, H., Hobble, E.A., Iversen, C.M., Jackson, R.B., Leppalammik-Jujansuu, J., Norby, R.J., Phillips, R.P., Pregitzer, K.S., Pritchard, S.G., Rewald, B., Zadworny, M., 2015. Redefining fine roots improves understanding of below-ground contributions to terrestrial biosphere processes. *New Phytol.* 207, 505–518.
- Moradi, A.B., Conesa, H.M., Robinson, B., et al., 2009. Neutron radiography as a tool for revealing root development in soil: capabilities and limitations. *Plant Soil* 318, 243–255.
- Moradi, A.B., Carminati, A., Vetterlein, D., Vontobel, P., Lehmann, E., Weller, U., Hopmans, J.W., Vogel, H.-J., Oswald, S.E., 2011. Three-dimensional visualization and quantification of water content in the rhizosphere. *New Phytol.* 192, 653–663.
- Moradi, A.B., Carminati, A., Lamparter, A., Woche, S.K., Bachmann, J., Vetterlein, D., Vogel, H.-J., Oswald, S.E., 2012. Is the rhizosphere temporarily water repellent? *Vadose Zone J.* 11 (3).
- Nakanishi, T.M., Okuni, Y., Hayashi, Y., Nishiyama, H., 2005. Water gradient profiles at bean plant roots determined by neutron beam analysis. *J. Radioanal. Nucl. Chem.* 264, 313–317.
- Naveed, M., Ahmed, M.A., Benard, P., Brown, L.K., George, T.S., Bengough, A.G., Roose, T., Koebernick, N., Hallett, P.D., 2019. Surface tension, rheology and

- hydrophobicity of rhizodeposits and seed mucilage influence soil water retention and hysteresis. *Plant Soil* 437, 65–81.
- Nazari, M., Bilyera, N., Banfield, C.C., Mason-Jones, K., Zarebanadkouki, M., Munene, R., Dippold, M.A., 2022. Soil, climate, and variety impact on quantity and quality of maize root mucilage exudation (in press). *Plant Soil*. <https://doi.org/10.1007/s11104-022-05669-x>.
- Oades, J.M., 1978. Mucilages at the root surface. *J. Soil Sci.* 29, 1–16.
- Oswald, S.E., Menon, M., Carminati, A., Vontobel, P., Lehmann, E., Schulin, R., 2008. Quantitative imaging of infiltration, root growth, and root water uptake via neutron radiography. *Vadose Zone J.* 7, 1035–1047.
- Pohlmeier, A., Javaux, M., Vereecken, H., Haber-Pohlmeier, S., Anderson, S.H., Hopmans, J.W., 2013. Magnetic resonance imaging techniques for visualization of root growth and root water uptake processes. In: Anderson, S.H., Hopmans, J.W. (Eds.), *Soil-water-root Processes: Advances in Tomography and Imaging*. SSSA Spec. Publ. SSSA, Madison, WI, pp. 137–156.
- Poirier, V., Roumet, C., Angers, D.A., Munson, A.D., 2018. Species and root traits impact macroaggregation in the rhizospheric soil of a Mediterranean common garden experiment. *Plant Soil* 424 (1–2), 289–302.
- Razavi, B.S., Zarebanadkouki, M., Blagodatskaya, E., Kuzyakov, Y., 2016. Rhizosphere shape of lentil and maize: spatial distribution of enzyme activities. *Soil Biol. Biochem.* 96, 229–237.
- Read, D.J., Boyd, R., 1986. Water relations of mycorrhizal fungi and their host plants. In: Ayres, P.G., Boddy, L. (Eds.), *Water, Fungi and Plants*. Press Syndicate and University of Cambridge, Cambridge, UK, pp. 287–303.
- Read, D.B., Bengough, A.G., Gregory, P.J., Crawford, J.W., Robinson, D., Scrimgeour, C. M., Young, I.M., Zhang, K., Zhang, X., 2003. Plant roots release phospholipid surfactants that modify the physical and chemical properties of soil. *New Phytol.* 157 (2), 315–326.
- Rewald, B., Ephrath, J.E., Rachmilevitch, S., 2011. A root is a root? Water uptake rates of citrus root orders. *Plant Cell Environ.* 34, 33–42.
- Roose, T., Keyes, S.D., Daly, K.R., et al., 2016. Challenges in imaging and predictive modeling of rhizosphere processes. *Plant Soil* 407, 9–38.
- Rudolph-Mohr, N., Vontobel, P., Oswald, S.E., 2014. A multi-imaging approach to study the root-soil interface. *Ann. Bot.* 114, 1779–1787.
- Rudolph-Mohr, N., Bereswill, S., Tötzke, C., et al., 2021. Neutron computed laminography yields 3D root system architecture and complements investigations of spatiotemporal rhizosphere patterns. *Plant Soil* 469, 489–501.
- Schlüter, S., Sheppard, A., Brown, K., Wildenschild, D., 2014. Image processing of multiphase images obtained via X-ray microtomography: a review. *Water Resour. Res.* 50, 3615–3639.
- Segal, E., Kushnir, T., Mualem, Y., Shani, U., 2008. Water uptake and hydraulics of the root hair rhizosphere. *Vadose Zone J.* 7 (3), 1027–1034.
- Tötzke, C., Kardjilov, N., Manke, I., Oswald, S.E., 2017. Capturing 3D water flow in rooted soil by ultra-fast neutron tomography. *Sci. Rep.* 7, 6192.
- Tötzke, C., Kardjilov, N., Hilger, A., et al., 2021. Three-dimensional in vivo analysis of water uptake and translocation in maize roots by fast neutron tomography. *Sci. Rep.* 11, 10578.
- Tumlinson, L.G., Liu, H., Silk, W.K., Hopmans, J.W., 2008. Thermal neutron computed tomography of soil water and plant roots. *Soil Sci. Soc. Am. J.* 72, 1234–1242.
- Venkatakrishnan, S., Ziabari, A., Hinkle, J., Needham, AW., Warren, JW., Bilheux, H.Z., 2021. Convolutional neural network based non-iterative reconstruction for accelerating neutron tomography. *Machine Learning Science and Technology* 2, 1–17.
- Warren, J.M., Brooks, J.R., Meinzer, F.C., Eberhart, J.L., 2008. Hydraulic redistribution of water from *Pinus ponderosa* trees to seedlings: evidence for an ectomycorrhizal pathway. *New Phytol.* 178, 382–394.
- Warren, J.M., Bilheux, H., Kang, M., Voisin, S., Cheng, C.-L., Horita, J., Perfect, E., 2013. Neutron imaging reveals internal plant water dynamics. *Plant Soil* 366, 683–693.
- Wells, C.E., Eissenstat, D.M., 2003. Beyond the roots of young seedlings: the influence of age and order on fine root physiology. *J. Plant Growth Regul.* 21, 324–334.
- Whalley, W.R., Riseley, B., Leeds-Harrison, P.B., Bird, N.R.A., Leech, P.K., Adderley, W. P., 2005. Structural differences between bulk and rhizosphere soil. *Eur. J. Soil Sci.* 56, 353–360.
- York, L.M., Carminati, A., Mooney, S.J., Ritz, K., Bennett, M.J., 2016. The holistic rhizosphere: integrating zones, processes, and semantics in the soil influenced by roots. *J. Exp. Bot.* 67 (12), 3629–3643.
- Zarebanadkouki, M., Kim, Y.X., Carminati, A., 2013. Where do roots take up water? Neutron radiography of water flow into the roots of transpiring plants growing in soil. *New Phytol.* 199, 1034–1044.
- Zarebanadkouki, M., Kroener, E., Kaestner, A., Carminati, A., 2014. Visualization of root water uptake: quantification of deuterated water transport in roots using neutron radiography and numerical modeling. *Plant Physiol.* 166, 487–499.
- Zarebanadkouki, M., Ahmed, M.A., Carminati, A., 2016. Hydraulic conductivity of the root-soil interface in sandy soil after drying and rewetting. *Plant Soil* 398, 267–280.
- Zarebanadkouki, M., Ahmed, M., Hedwig, C., Benard, P., Kostka, S.J., Kastner, A., Carminati, A., 2018. Rhizosphere hydrophobicity limits root water uptake after drying and subsequent rewetting. *Plant Soil* 1–13.
- Zwieniecki, M.A., Thompson, M.V., Holbrook, N.M., 2003. Understanding the hydraulics of porous pipes: tradeoffs between water uptake and root length utilization. *J. Plant Growth Regul.* 21, 315–323.